Rapid Communications

Universal scaling of the thermalization time in one-dimensional lattices

Weicheng Fu, Yong Zhang, and Hong Zhao*

Department of Physics and Jiujiang Research Institute, Xiamen University, Xiamen 361005, Fujian, China

(Received 23 December 2018; revised manuscript received 20 May 2019; published 15 July 2019)

We show that, in the thermodynamic limit, a one-dimensional (1D) nonlinear lattice can always be thermalized for arbitrarily small nonlinearity, thus proving the equipartition theorem for a class of systems. Particularly, we find that in the lattices with nearest-neighbor interaction potential $V(x) = x^2/2 + \lambda x^n/n$ with $n \geqslant 4$, the thermalization time, $T_{\rm eq}$, follows a universal scaling law; i.e., $T_{\rm eq} \propto \lambda^{-2}\epsilon^{-(n-2)}$, where ϵ is the energy per particle. Numerical simulations confirm that it is accurate for an even n, while a certain degree of deviation occurs for an odd n, which is attributed to the extra vibration modes excited by the asymmetric interaction potential. This finding suggests that although the symmetry of interactions will not affect the system reaching equipartition eventually, it affects the process toward equipartition. Based on the scaling law found here, a unified formula for the thermalization time of a 1D general nonlinear lattice is obtained.

DOI: 10.1103/PhysRevE.100.010101

Introduction. The equipartition theorem assumes that arbitrarily small nonlinearity is enough to thermalize a macroscopic thermodynamic system, i.e., the energy will be equally distributed among the Fourier modes. It is the foundation of statistical physics. The pioneering numerical experiments by Fermi, Pasta, Ulam, and Tsingou (FPUT) [1,2], showed very little tendency toward equipartition of energy among the modes, known as the FPUT paradox [1]. Their seminal work has stimulated a huge amount of research (see Refs. [3–13], and references therein). Extensive numerical simulations have shown clear evidence that there is an energy threshold above which the FPUT system reaches a fast thermalized state [14–17]. However, whether a system can be generally thermalized for arbitrarily small nonlinearity has not been settled clearly due to the difficulty of rigorous mathematical proof [3].

Recently, the wave turbulence (WT) theory [18–23] has been applied to attack this problem [24–26] and opens a new path toward a rigorous proof of the outstanding equipartition hypothesis. This theory [24] assumes that, in the weakly nonlinear regime, the long-time dynamics of a one-dimensional (1D) lattice is determined by exact multiwave resonances, and the thermalization is governed by the nontrivial resonances. The umklapp process is a key nontrivial resonance, since it causes the irreversible transfer of energy due to the flipover of wave vectors over the edge of the Brillouin zone. When all the normal modes are interconnected by the nontrivial resonances, the equipartition may be expected. Finally, it predicts that the thermalization time $T_{\rm eq}$ is inversely proportional to the square of the coupling coefficient of the dominant nontrivial resonances. Based on this theory, landmark progress has been made for the lattices with Hamiltonian

$$H = \sum_j \frac{p_j^2}{2} + \frac{(q_{j+1} - q_j)^2}{2} + \frac{\lambda}{n}(q_{j+1} - q_j)^n \qquad (1)$$

for the special cases of $n = 3$ (FPUT-α model) [24] and $n = 4$ (FPUT-β model) [25], where p_j and q_j are, respectively, the momentum and the displacement from the equilibrium position of the jth particle, and λ is a positive constant. In these two models with small finite size, it has been found that the first nontrivial resonances correspond to six-wave interactions, which lead to $T_{\rm eq} \propto \lambda^{-8}\epsilon^{-4}$ [24] and $T_{\rm eq} \propto \lambda^{-4}\epsilon^{-4}$ [25], respectively, where ϵ is the energy density (i.e., the energy per particle). The power-law behavior implies that the equipartition state can always be reached for arbitrarily small nonlinearity.

However, some essential problems are still open; e.g., whether this conclusion can be extended to a general 1D lattice in the thermodynamic limit and whether there is a universal scaling law for the equipartition time. The first issue has been discussed in Refs. [24,25], where the authors have conjectured that the four-wave resonances will dominate thermalization in the thermodynamic limit for the FPUT-α and FPUT-β models, which results in $T_{\rm eq} \propto \lambda^{-4}\epsilon^{-2}$ [24] and $T_{\rm eq} \propto \lambda^{-2}\epsilon^{-2}$ [25], respectively. In a more recent work [27], numerical evidence has been provided. Meanwhile, for the discrete Klein-Gordon model, it has been shown with the WT theory that the equipartition can be achieved in the thermodynamic limit [26]. Note that the Klein-Gordon model is subject to an on-site potential and thus does not belong to the FPUT class. The second issue has not been studied systematically, though various scaling laws of equipartition time have been proposed previously for different scenarios [28–31].

In this Rapid Communication, based on the WT theory, we show that there is *a universal scaling law* of the thermalization time for the models given by Eq. (1) *in the thermodynamic limit*, i.e., $T_{\rm eq} \propto \lambda^{-2}\epsilon^{-(n-2)}$ for $n \geqslant 4$. Our key finding is that the lowest order resonances, i.e., the n-wave resonances for the model with a power-law potential of power n, survive in the thermodynamic limit and are responsible for thermalization, except when $n = 3$. Our extensive numerical simulations confirm that this scaling is accurate for an even n, but is

*zhaoh@xmu.edu.cn

smaller for an odd n. The deviation decreases with the increase of n. This deviation is attributed to the extra vibration modes excited by the asymmetric interaction potential, thus the WT theory fails to capture them.

Theoretical analysis. We consider a lattice of $N+1$ particles with fixed ends ($q_0 = q_N = 0$) such that there are $N-1$ moving particles in between. The displacement of the jth particle can be written in terms of normal modes as

$$q_j = i \sum_{k=-N}^{N} \frac{Q_k}{\omega_k} e^{-ijk\pi/N}, \tag{2}$$

where $\omega_k = 2\left|\sin\left(\frac{k\pi}{2N}\right)\right|$ is the dispersion relation, and Q_k is the amplitude of the kth normal mode [32]. The boundary conditions, along with the reality of q_j, i.e., $q_j = q_j^*$, impose the constraint to the modes that $Q_k = Q_{-k} = Q_k^*$, and $Q_N = Q_{-N} = Q_0 = 0$. It is convenient to introduce the dimensionless complex amplitude of the kth normal mode

$$a_k = \frac{\sqrt{N}Q_k + i\omega_k P_k/\sqrt{N}}{\epsilon^{1/2}\sqrt{2\omega_k}}, \tag{3}$$

where $P_k = \partial H/\partial \dot{Q}_k$ is the canonically conjugate momentum. Then, the Hamiltonian (1) can be rewritten in the dimensionless form ($\tilde{H} = H/\epsilon$):

$$\tilde{H} = \sum_k \omega_k a_k a_k^* + \frac{\lambda\epsilon^{(n-2)/2}}{n} \sum_{k_1,\ldots,k_n} \Phi_{k_1}^{k_n} \delta(k_{1,n}) \prod_{l=1}^{n} \left(a_{k_l} + a_{k_l}^*\right), \tag{4}$$

where $\Phi_{k_1}^{k_n} = \frac{N}{(2N)^{n/2}} \frac{\sqrt{\prod_{l=1}^{n}\omega_{k_l}}}{\mathrm{sgn}\left(\prod_{l=1}^{n} k_l\right)}$ is an interaction tensor coefficient, and $\delta(k_{1,n})$ gives the n-wave resonant condition for the wave vectors [22], i.e., $k_1 \pm k_2 \pm \cdots \pm k_n = 0$. Whether the function sign takes $+1$ or -1 depends on the type of the n-wave process. Then, the equation of motion for the k_1th complex normal mode reduces to

$$i\frac{\partial a_{k_1}}{\partial t} = \omega_{k_1} a_{k_1} + \lambda\epsilon^{(n-2)/2} \sum_{k_2,\ldots,k_n} \Phi_{k_1}^{k_n} \delta(k_{1,n}) \prod_{l=2}^{n} \left(a_{k_l} + a_{k_l}^*\right). \tag{5}$$

From this equation we see that the nonlinear interactions are manifested as an n-wave scattering process. To evaluate the equipartition time, we introduce the wave action spectral density $A_i\delta_i^j = \langle a_{k_i} a_{k_j}^* \rangle$ following the WT theory [24,25], where the brackets indicate the ensemble average and δ_i^j is the Kronecker delta. Based on the WT theory [22], one can derive the n-wave kinetic equation

$$\dot{A}_1 = 4\pi\lambda^2\epsilon^{n-2} \int_{-\pi}^{\pi} \left|\Phi_{k_1}^{k_n}\right|^2 \mathscr{F}(A_{1,n}) \delta(k_{1,n}) \delta(\omega_{1,n}) dk_2 \cdots dk_n, \tag{6}$$

where $\mathscr{F}(A_{1,n})$ is a function of $A_1, A_2, \ldots, A_n$, and $\delta(\omega_{1,n})$ gives the n-wave resonant condition for the frequencies, i.e., $\omega_{k_1} \pm \omega_{k_2} \pm \cdots \pm \omega_{k_n} = 0$ (see the Supplemental Material [33] and Ref. [22] for details). The summation of the wave vector from $-N$ to N is replaced by an integral from $-\pi$ to π on the reduced wave vector because the wave numbers in the Fourier space become dense and continuous in the thermodynamic limit.

Based on the evolution equation (6), $T_{\mathrm{eq}} \propto \lambda^{-2}\epsilon^{-(n-2)}$ holds when the nontrivial n-wave resonances exist and dominate thermalization. In the thermodynamic limit, the wave vectors become dense and the resonant conditions are not forbidden by the dispersion relation for $n \geqslant 4$; therefore, the n-wave resonant solutions may exist [19]. In addition, considering the fact that any frequency will broaden due to the nonlinearity, the resonant n tuplets are interconnected.

For $n = 3$, i.e., the FPUT-α model, the three-wave resonances are forbidden because of the shape of the dispersion relation [19,24]. Hence, for this model one has to introduce a new canonical transformation to consider higher order interactions. We agree with the argument in Ref. [24] that the four-wave resonances dominate the thermalization in the thermodynamic limit, which leads to $T_{\mathrm{eq}} \propto \lambda^{-4}\epsilon^{-2}$.

Such an approach can be extended to more general symmetric potentials, $V(x) = |x|^d/d$, with $d = m_1/m_2 > 2$ and m_1 and m_2 are coprimes. This is because the potential can be rewritten in terms of normal modes,

$$\sum_j |q_j - q_{j-1}|^{m_1/m_2} = \sum_j \left[\sum_{k_1,\ldots,k_{2m_1}} \frac{Q_{k_1} Q_{k_2} \cdots Q_{k_{2m_1}}}{\mathrm{sgn}\left(k_1 k_2 \cdots k_{2m_1}\right)} e^{i\pi\left(\frac{1}{2}-j\right)(k_1+\cdots+k_{2m_1})/N} \right]^{1/2m_2}, \tag{7}$$

and the equation of motion can be obtained similarly. Equation (7) indicates that the lowest number of waves participating in the scattering process is $2m_1$ in a model with exponent d, and $2m_1 \geqslant 4$ since $m_2 \geqslant 1$. Thus, the thermalization time $T_{\mathrm{eq}} \propto \lambda^{-2}\epsilon^{-(d-2)}$ for such symmetric models only if the $2m_1$-wave resonances exist and dominate thermalization in the thermodynamic limit.

Numerical experiments. Any numerical simulation is performed with a finite system, and therefore, the wave numbers are discrete in principle. However, because of the nonlinearity, each frequency corresponds to a spectral peak of a nonzero width. Thus near-resonance interactions [34] can occur. This allows us to observe the predictions of the WT theory as long as the system is large enough. In practical simulations, once the results no longer change with the further increase of the size, the thermodynamic limit is considered to have been approached.

We adopt the method presented in Ref. [30] to calculate equipartition time. The normal modes of a 1D lattice of $N+1$ particles are $Q_k = \sqrt{2/N}\sum_{j=1}^{N} q_j \sin(jk\pi/N)$, $P_k = \sqrt{2/N}\sum_{j=1}^{N} p_j \sin(jk\pi/N)$. The energy of the kth normal mode is $E_k = (P_k^2 + \omega_k^2 Q_k^2)/2$. The indicator of thermalization, $\xi(t) = \tilde{\xi}(t)\frac{e^{\eta(t)}}{N/2}$, is adopted, where $\eta(t) = -\sum_{k=N/2}^{N} w_k(t)\log[w_k(t)]$ is the spectral entropy, in which $w_k(t) = \frac{\bar{E}_k(t)}{\sum_{l=N/2}^{N}\bar{E}_l(t)}$, $\tilde{\xi}(t) = \frac{\sum_{k=N/2}^{N}\bar{E}_k(t)}{\frac{1}{2}\sum_{1\leqslant k\leqslant N}\bar{E}_k(t)}$, and $\bar{E}_k(T) = \frac{1}{(1-\mu)T}\int_{\mu T}^{T} E_k[P(t), Q(t)]dt$ is the average energy of the kth mode. Here, μ is a free parameter that controls the size of the time window for averaging. The thermalization time is defined by $\xi(T_{\mathrm{eq}}) = C$ with $C = 1/2$ as in Refs. [6,30], and it

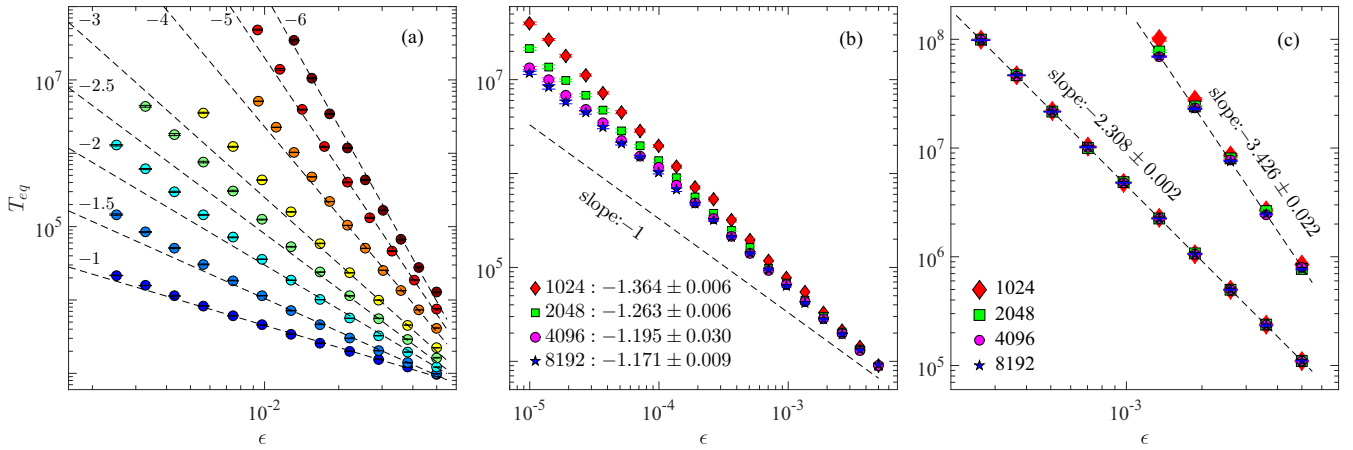

FIG. 1. The equipartition time T_{eq} as a function of energy density ϵ in log-log scale. (a) For symmetric models $V(x) = |x|^d/d$ with $d = 3, 7/2, 4, 9/2, 5, 6, 7, 8$ from bottom to top, and dashed lines with slope $2 - d$ are drawn for reference, fixed $N = 2048$. (b) For the symmetric model $d = 3$ with different size $N = 1024, 2048, 4096, 8192$ from top to bottom. The slopes of best linear fit are listed in the plot, and a dashed line is drawn for reference. (c) For asymmetric models $n = 3$ (bottom) and $n = 5$ (top) with different size, and dashed lines are the best linear fit corresponding to $N = 8192$.

has been verified that the scaling exponent does not depend on the specific value of C.

For the numerical integration of Hamilton's canonical equations, we used the eighth-order Yoshida method [35]. To suppress fluctuations, the average is done over 60 phases uniformly distributed in $[0, 2\pi]$.

Note that $H' = \epsilon H$ under the scaling transformation $q' = q\epsilon^{1/2}$ for the power-potential models (1); hence, the nonlinear parameter λ and the energy density ϵ has a rigid scaling relation $\lambda' = \lambda\epsilon^{(n-2)/2}$. Therefore, it is equivalent to study the scaling of λ by fixing ϵ or that of ϵ by fixing λ. Here, we perform the latter with fixed $\lambda = 1$. Figure 1(a) shows the results for several symmetric power potentials with $N = 2048$. It shows that the scaling $T_{eq} \propto \epsilon^{-(d-2)}$ agrees with the data very well, although a slight deviation can be recognized which has been confirmed to be a finite-size effect. This finite-size effect is shown in Fig. 1(b) by taking the case of $d = 3$ as an example, where we can see that the larger the system size, the smaller the deviation; meanwhile, the lower the energy density, the larger the size must be for converging to the theoretical scaling. This plot also indicates that, in the thermodynamic limit, the theoretical prediction applies to arbitrarily small nonlinearity.

Figure 1(c) presents the results for models with $n = 3$ and $n = 5$. Best fitting gives $T_{eq} \propto \epsilon^{-2.31}$ and $T_{eq} \propto \epsilon^{-3.43}$, respectively. The finite-size effect is negligible compared to that of symmetric potentials. The result for $n = 3$ approaches the four-wave resonance prediction of $T_{eq} \propto \epsilon^{-2}$, while that for $n = 5$ is close to the five-wave resonance prediction, i.e., $T_{eq} \propto \epsilon^{-3}$.

Why the symmetry of interactions makes a difference. To reveal why there is a deviation from the WT theory for models with an odd n, we study the power spectrum of the time series of momentum of a particle using the fast Fourier transform (the result does not depend on the specific choice of the particle). Figures 2(a)–2(c) show the results for the FPUT-α model with three sizes, $N = 17$, 65, and 1025, respectively, at the fixed energy density $\epsilon = 3\times10^{-3}$. For the sake of clarity, only the first two lowest frequency modes are plotted. Figures 2(a) and 2(b) show that there are many regularly distributed small peaks between two neighboring normal modes in the asymmetric case ($n = 3$), but they are absent in the symmetric case ($d = 3$). With the further increase of the lattice size, the small peaks disappear. However, the difference is still obvious between the symmetric and asymmetric models: the phonon peaks remain symmetric for the former while they become asymmetric for the latter. Obviously, it is the symmetry of the interaction potential that makes the difference.

By calculating the power spectrum of the normal modes, i.e., taking the Fourier transform of $a_k(t)$ to obtain $a_k(\omega)$, we find that the number of small peaks is governed by the system size. Figures 3(a) and 3(b) show the results of $a_1(\omega)$ with $N = 6$ and 10 for $n = 3$, 5, 7, respectively. Figure 3(c) shows the height of the first small peak as a function of the energy density. These figures indicate that, on one hand, the height of small peaks decrease in a power-law manner with the decrease

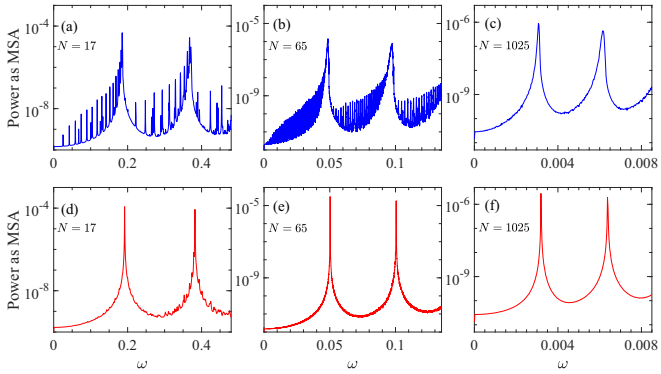

FIG. 2. Power spectra of the time series of momentum normalized by mean squared amplitude (MSA). (a)–(c) for asymmetric model ($n = 3$). (d)–(f) for symmetric model ($d = 3$). Figures from left to rihgt correspond to the lattice size $N = 17$, 65, and 1025, respectively. $\epsilon = 0.003$ is fixed.

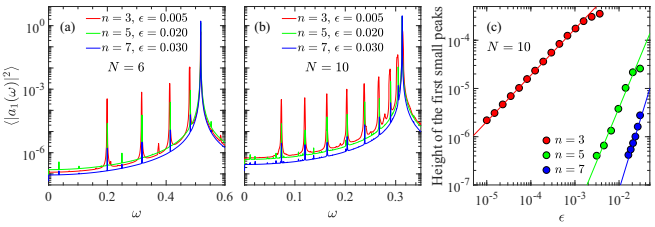

FIG. 3. (a) and (b) $\langle |a_1(\omega)|^2 \rangle$ vs ω for asymmetric power potential with $n = 3$ (red line), $n = 5$ (green line), and $n = 7$ (blue line), respectively. (c) The height of the first small peak vs energy density. Solid lines are drawn for reference.

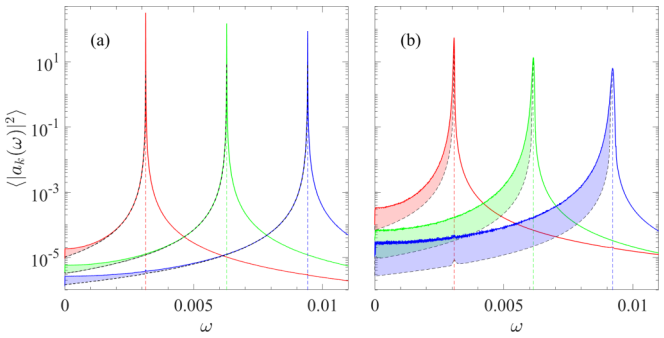

FIG. 4. $\langle |a_k(\omega)|^2 \rangle$ vs ω for $k = 1$ (red line), $k = 2$ (green line), and $k = 3$ (blue line). (a) For the symmetric power potential with $d = 3$. (b) For the asymmetric power potential with $n = 3$. In order to show the asymmetry of a peak, the mirror image of its right profile line with respect to the vertical dashed line passing through the summit is drawn (black dashed line); the area (shadowed) between which, and the left profile line, thus visualizes the asymmetry. $\epsilon = 10^{-3}$ is fixed.

of the energy density, implying that they exist in arbitrarily small nonlinearity; on the other hand, we find that at the same energy density, the peaks for different n can be enormously different in amplitude. For this reason, in Figs. 3(a) and 3(b) we plot the results for different n with different energy density instead. We see that there are two types of small peaks. The first type is independent of n. They appear at the fixed positions, and their number, $N-2$, increases as N. Another type appears occasionally at different positions for different n [Fig. 3(a)]. This type of peaks disappear eventually at big N [Fig. 3(b)]. On the other hand, since ω_1 decreases with the increase of N as $\omega_1 = 2\sin\frac{\pi}{2N}$, the average distance between two adjacent peaks decreases as $\Delta\omega_1 = \frac{2}{N-2}\sin\frac{\pi}{2N}$. For sufficiently large N, $\Delta\omega_1 \sim \pi/N^2$. This number is contributed just by the first normal mode. Thus, the density of the extra peaks in Fig. 2 is much bigger due to the contribution of other normal modes.

As a result, neighboring small peaks can be infinitely close to each other with the increase of N. In addition, due to the nonlinearity, each peak must have a nonzero width. Following the dynamics theory [36,37], the resonances among near peaks must occur in this case. The resonances may lead to the peaks merging with each other, and one can expect that at sufficiently large N the left-hand side line of the phonon peak will develop into the envelope of the merged peaks.

To check this prediction, in Fig. 4(a) we show the power spectrum for several low-frequency normal modes, $a_1(\omega)$, $a_2(\omega)$, and $a_3(\omega)$, respectively, for both the symmetric and asymmetric models with $N = 1025$. We see that the symmetric model keeps the usual symmetric Lorentzian line shape for the phonon peaks, while in the asymmetric model the phonon peak has an asymmetric line shape—it is the merge of the extra small peaks that leads to such a result. The shadow area is an indication of the deviation of phonon peaks from the Lorentzian line shape.

With the above analysis we can explain the simulation results. First, the normal modes can well capture the dynamics of the system with a symmetric interaction potential in the thermodynamic limit since they are the unique energy carriers. Therefore, the WT theory works for such a system. Second, for a sufficiently small lattice with asymmetric power function potential, the small peaks are sparse and isolated. Despite their existence, their influence on the thermalization time is negligible; this is why the simulation results still agree with the theoretical prediction for a FPUT-α model [24]. Third, as the system size increases, the small peaks become closer to each other. For large N, the spectrum becomes continuous due to the overlap; it appears in effect as the envelope of the dense small peaks and the normal mode peaks. In this way, an additional transport channel opens, and one can expect that it contributes to the irreversible energy mixing, which results in the deviations. Finally, the amplitudes of small peaks are smaller at the fixed energy density for models with large power of n. Therefore, as n increases, the deviation decreases accordingly.

General formula. A general interaction potential can be expanded in the Taylor series with respect to its equilibrium position, i.e., $V(x) = \sum_2^\infty V^{(n)}(0)x^n/n!$ (note that the linear term vanishes at the equilibrium point and the constant term is futile). The corresponding equation of motion is similar to Eq. (5), with an expanding series of n-wave coupling terms. In the thermodynamic limit, four-wave resonances will be excited by the term of $n = 3$, and other n-wave resonances will be excited by other terms of n existing simultaneously. According to the condensed matter physics theory, if multiple independent scattering processes coexist, one can apply the Matthiessens rule [38] to integrate their contributions. For example, when the scattering induced by lattice phonons and by impurities can be considered independent, the true average relaxation time τ can be estimated as $1/\tau = 1/\tau_{\text{lattice}} + 1/\tau_{\text{impurities}}$, where τ_{lattice} and $\tau_{\text{impurities}}$ represent the relaxation times if there is only the lattice scattering or only the impurity scattering. In our case here, in the weakly nonlinear region, the scattering sources should be multiwave resonances. If we assume that the scatterings of different n-wave resonances are independent, the combined relaxation time T_{eq} can be estimated following the Matthiessen's rule as

$$\frac{1}{T_{\text{eq}}} = \frac{1}{T_{\text{eq}}^{(3)}} + \frac{1}{T_{\text{eq}}^{(4)}} + \cdots, \tag{8}$$

where $T_{\text{eq}}^{(n)}$ represents the relaxation time contributed by the potential term with power exponent n.

We check this formula with two examples. The first one is for $V(x) = \frac{1}{2}x^2 + \frac{\alpha}{3}x^3 + \frac{1}{6}x^6$, where α is used to adjust the relative weights of the two anharmonic terms. Here we

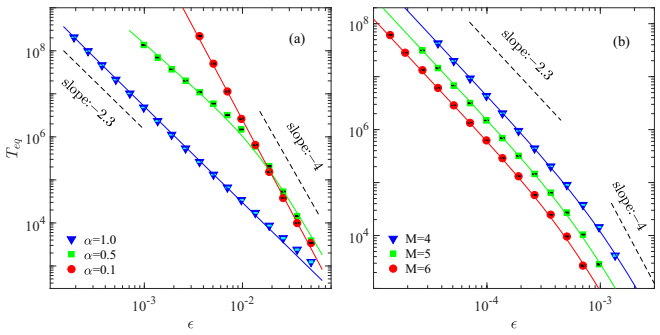

FIG. 5. The equipartition time $T_{\rm eq}$ as a function of energy density ϵ in log-log scale for (a) the cubic plus six-power potential model with different α, and (b) the LJ model with different M. Solid lines are best fitting with Eq. (8), and $n = 3, 6$ for (a); $n = 3, 4, 5, 6$ for (b). Dashed lines are drawn for reference.

introduce the sixth-order nonlinearity instead of the fourth since the scaling exponents for $n = 3$ and $n = 4$ are too close ($T_{\rm eq}^{(3)} \propto \epsilon^{-2.31}$ and $T_{\rm eq}^{(4)} \propto \epsilon^{-2}$, respectively), which makes it difficult to observe an obvious variation of the scaling exponent in simulations. Figure 5(a) shows the numerical results for $\alpha = 0.1,\ 0.5$, and 1.0, respectively. We see that the four-wave and six-wave resonances dominate the thermalization process in the two extremes of $\alpha = 1$ and 0.1, respectively. For a moderate cubic potential there appears a crossover. In all three cases, Eq. (8) can well fit the numerical results when we input $T_{\rm eq}^{(3)} = c_3\epsilon^{-2.31}$ and $T_{\rm eq}^{(6)} = c_6\epsilon^{-4}$ with proper weight parameters c_3 and c_6.

Our second example is the Lennard-Jones (LJ) model [39] with $V(x) = \frac{1}{2M^2}[\frac{1}{(1+x)^{2M}} - \frac{2}{(1+x)^M} + 1]$, which is frequently adopted for modeling a real lattice system. Here M is an integer, and $M = 6$ is the case considered the most often. Note that the Taylor series expansion of the LJ potential involves various power-potential terms. The numerical results are presented in Fig. 5(b). It shows that Eq. (8) fits the numerical results well for all values of M we have ever tried.

Conclusion. In summary, in models with interaction potential $V(x) = x^2/2 + \lambda x^n/n$, the n-wave nontrivial resonances dominate thermalization in the thermodynamic limit and lead to the universal scaling law of $T_{\rm eq} \propto \lambda^{-2}\epsilon^{-(n-2)}$ for $n \geqslant 4$. Such a scaling law also exists in symmetric models with $V(x) = x^2/2 + \lambda|x|^d/d$, where d is rational and $d > 2$. Only for $n = 3$ does one need a further canonical transformation to find higher-order resonances. Extensive numerical simulations confirm that this scaling holds perfectly in the symmetric models. It holds approximately for the asymmetric power potentials, but the deviation is slight.

Our study covers the most general class of 1D systems without on-site potential since any interaction potential can be expanded in terms of power potentials. Moreover, based on our scaling law and inspired by Matthiessen's rule, we have derived a formula of $T_{\rm eq}$ for a general interaction potential.

In seeking the underlying mechanism of deviation from the universal scaling law in asymmetric models, we find that a large number of extra vibration modes can be excited by the asymmetric interaction potential, and resonances may take place between them in a large system, which leads to the deviation. Furthermore, the extra vibration modes make phonon peaks asymmetrically broadened. This finding provides a new explanation for the asymmetric line shape of phonon spectra that has been widely reported in various condensed matter studies [40–47]. It is possible that more than one mechanism is responsible for this phenomenon [43–47]. The resonance between the extra vibration modes generated by the asymmetric interaction potential may be a microscopic mechanism for the widely observed asymmetric line shape of phonon peaks. Namely, it is the asymmetric interparticle interaction that leads to the asymmetric line shape of the phonon peaks. As asymmetric interactions are ubiquitous in real materials, this mechanism could be very fundamental.

Acknowledgment. We are grateful to Jiao Wang for fruitful discussions. We acknowledge support by NSFC (Grant No. 11335006).

[1] E. Fermi, J. Pasta, and S. Ulam, Los Alamos Scientific Laboratory, Report No. LA-1940, 1955.
[2] T. Dauxois, Phys. Today **61**(1), 55 (2008).
[3] *The Fermi-Pasta-Ulam Problem*, edited by G. Gallavotti, Lecture Notes in Physics Vol. 728 (Springer-Verlag, Berlin, 2008).
[4] M. Wu and C. E. Patton, Phys. Rev. Lett. **98**, 047202 (2007).
[5] A. Mussot, A. Kudlinski, M. Droques, P. Szriftgiser, and N. Akhmediev, Phys. Rev. X **4**, 011054 (2014).
[6] Z. Zhang, C. Tang, and P. Tong, Phys. Rev. E **93**, 022216 (2016).
[7] C. Bao, J. A. Jaramillo-Villegas, Y. Xuan, D. E. Leaird, M. Qi, and A. M. Weiner, Phys. Rev. Lett. **117**, 163901 (2016).
[8] C. Danieli, D. K. Campbell, and S. Flach, Phys. Rev. E **95**, 060202(R) (2017).
[9] M. Guasoni, J. Garnier, B. Rumpf, D. Sugny, J. Fatome, F. Amrani, G. Millot, and A. Picozzi, Phys. Rev. X **7**, 011025 (2017).
[10] A. Mussot, C. Naveau, M. Conforti, A. Kudlinski, F. Copie, P. Szriftgiser, and S. Trillo, Nat. Photon. **12**, 303 (2018).
[11] Y. Wang, Z. Zhu, Y. Zhang, and L. Huang, Phys. Rev. E **97**, 012143 (2018).
[12] Y. Wang, Z. Zhu, Y. Zhang, and L. Huang, Appl. Phys. Lett. **112**, 111910 (2018).
[13] D. Pierangeli, M. Flammini, L. Zhang, G. Marcucci, A. J. Agranat, P. G. Grinevich, P. M. Santini, C. Conti, and E. DelRe, Phys. Rev. X **8**, 041017 (2018).
[14] R. Livi, M. Pettini, S. Ruffo, M. Sparpaglione, and A. Vulpiani, Phys. Rev. A **31**, 1039 (1985).
[15] J. Ford, Phys. Rep. **213**, 271 (1992).
[16] L. Casetti, M. Cerruti-Sola, M. Pettini, and E. G. D. Cohen, Phys. Rev. E **55**, 6566 (1997).
[17] J. De Luca, A. J. Lichtenberg, and S. Ruffo, Phys. Rev. E **60**, 3781 (1999).

[18] V. E. Zakharov, V. S. L'Vov, and G. Falkovich, *Kolmogorov Spectra of Turbulence I. Wave Turbulence* (Springer, Berlin, 1992).
[19] A. J. Majda, D. W. McLaughlin, and E. G. Tabak, J. Nonlinear Sci. **7**, 9 (1997).
[20] V. Zakharov, P. Guyenne, A. Pushkarev, and F. Dias, Phys. D (Amsterdam, Neth.) **152-153**, 573 (2001).
[21] V. Zakharov, F. Dias, and A. Pushkarev, Phys. Rep. **398**, 1 (2004).
[22] *Wave Turbulence*, edited by S. Nazarenko, Lecture Notes in Physics Vol. 825 (Springer-Verlag, Berlin, 2011).
[23] P. Sagaut and C. Cambon, *Homogeneous Turbulence Dynamics*, 2nd ed. (Springer, New York, 2018).
[24] M. Onorato, L. Vozella, D. Proment, and Y. V. Lvov, Proc. Natl. Acad. Sci. USA **112**, 4208 (2015).
[25] Y. V. Lvov and M. Onorato, Phys. Rev. Lett. **120**, 144301 (2018).
[26] L. Pistone, M. Onorato, and S. Chibbaro, Europhys. Lett. **121**, 44003 (2018).
[27] L. Pistone, S. Chibbaro, M. Bustamante, Y. L'vov, and M. Onorato, arXiv:1812.08279.
[28] J. DeLuca, A. J. Lichtenberg, and S. Ruffo, Phys. Rev. E **51**, 2877 (1995).
[29] L. Berchialla, A. Giorgilli, and S. Paleari, Phys. Lett. A **321**, 167 (2004).
[30] G. Benettin and A. Ponno, J. Stat. Phys. **144**, 793 (2011).
[31] G. Benettin, H. Christodoulidi, and A. Ponno, J. Stat. Phys. **152**, 195 (2013).
[32] R. Bivins, N. Metropolis, and J. R. Pasta, J. Comput. Phys. **12**, 65 (1973).
[33] See Supplemental Material at http://link.aps.org/supplemental/10.1103/PhysRevE.100.010101 for additional theoretical analysis.
[34] B. Gershgorin, Y. V. Lvov, and D. Cai, Phys. Rev. Lett. **95**, 264302 (2005).
[35] H. Yoshida, Phys. Lett. A **150**, 262 (1990).
[36] F. M. Izrailev and B. V. Chirikov, Dokl. Akad. Nauk SSSR **166**, 57 (1966) [Sov. Phys. Dokl. **11**, 30 (1966)].
[37] B. V. Chirikov, Phys. Rep. **52**, 263 (1979).
[38] G. P. Srivastava, *The Physics of Phonons* (Hilger, Bristol, 1990).
[39] S. Chen, Y. Zhang, J. Wang, and H. Zhao, J. Stat. Mech. (2016) 033205.
[40] A. S. Barker, Phys. Rev. **165**, 917 (1968).
[41] B. Li, D. Yu, and S.-L. Zhang, Phys. Rev. B **59**, 1645 (1999).
[42] M. Rajalakshmi, A. K. Arora, B. S. Bendre, and S. Mahamuni, J. Appl. Phys. **87**, 2445 (2000).
[43] P. T. Araujo, D. L. Mafra, K. Sato, R. Saito, J. Kong, and M. S. Dresselhaus, Phys. Rev. Lett. **109**, 046801 (2012).
[44] Y. Gao and P. Yin, Sci. Rep. **7**, 43602 (2017).
[45] I. Niehues, R. Schmidt, M. Druppel, P. Marauhn, D. Christiansen, M. Selig, G. Berghauser, D. Wigger, R. Schneider, L. Braasch *et al.*, Nano Lett. **18**, 1751 (2018).
[46] M. C. Ceballoschuc, C. M. Ramoscastillo, J. J. Alvaradogil, G. Oskam, and G. Rodriguezgattorno, J. Phys. Chem. C **122**, 19921 (2018).
[47] B. Xu, H. Xiao, B. Gao, Y. H. Ma, G. Mu, P. Marsik, E. Sheveleva, F. Lyzwa, Y. M. Dai, R. P. S. M. Lobo, and C. Bernhard, Phys. Rev. B **97**, 195110 (2018).